

Journal of
Mechanics of
Materials and Structures

**PLASTIC YIELD AND COLLAPSE MECHANISM OF PLANAR
LATTICE STRUCTURES**

Yihui Zhang, Zhenyu Xue, Xinming Qiu and Daining Fang

Volume 3, N° 7

September 2008



mathematical sciences publishers

PLASTIC YIELD AND COLLAPSE MECHANISM OF PLANAR LATTICE STRUCTURES

YIHUI ZHANG, ZHENYU XUE, XINMING QIU AND DAINING FANG

Lattice structures possess a huge potential for energy absorbing applications, and the postinitial collapse region should be analyzed with respect to design principles in such cases. This paper presents an analytical method to calculate the ultimate yield surfaces of statically indeterminate planar lattice structures, based on the assessment of static equilibrium of the unit cell before and after initial yielding. The material of the unit cell wall is assumed to be elastic, perfectly plastic. Three statically indeterminate planar lattice structures: the diamond cross cell, the statically-indeterminate square cell (SI-square cell), the new Kagome cell (N-Kagome), are analyzed. The parametric studies reveal the roles of various geometrical parameters on the performance of each structure. The SI-square cell is utilized as an example to demonstrate the evolution of structural yielding, thus providing an insight into the collapse mode of lattice structures. Furthermore, the stress-strain relationships of the SI-square and N-Kagome cells are also calculated, and the effective constitutive relations of both lattices are found to be linearly hardening, which is validated by finite element (FE) simulations.

1. Introduction

Recently, lightweight structures, including metal foams, metallic sandwiches with various core topologies, and lattice structures, have been widely used in engineering applications [Gibson and Ashby 1997; Ashby et al. 2000; Smith et al. 2001; Xue and Hutchinson 2003; 2004; 2006; Hutchinson and Xue 2005] for their superior properties of high specific stiffness and strength, most effective energy absorption, shock mitigation, and heat insulation. A lattice structure consists of periodically patterned trusses or sheets which provide large interstructural spaces, thus significantly enhancing the mechanical performance of the structure compared with the equivalent solid plate of same weight. Furthermore, the periodic cellular structures possess far superior specific strengths compared with disordered structures such as Voronoi honeycombs [Fazekas et al. 2002] or less ordered open or closed cell metallic foams [Doyoyo and Wierzbicki 2003]. Two-dimensional lattice structures possess configurations with regular and periodic microstructures in a plane and remain the same along the normal direction of the plane. Because two-dimensional lattice structures are attractive for use as cores in lightweight sandwich beams or plates, for load carrying, energy-absorption, and packaging applications, various aspects of their mechanical and thermal behaviors have received significant attention [Gibson and Ashby 1997; Chen et al. 1999; Evans et al. 2001; Hayes et al. 2004; Fleck and Qiu 2007].

Keywords: planar lattice structures, plasticity, yield surface, structural collapse.

The authors are grateful for the support by National Natural Science Foundation of China under grants #10632060 and #10502027. Supported by the Special Funds for the Major State Basic Research Projects of China (#G2003CB615603, #G2006CB601202) is also acknowledged.

Yielding is generally premonitory of structural collapse for lattice structures, and so a comprehensive understanding of lattice yielding behavior is indispensable for engineering applications. Previous studies on yielding behavior of cellular structures were mainly focused on the yielding criterion and the continuum constitutive relations, and employed the phenomenological and micromechanics methods in the analysis of the periodic unit cell. Deshpande and Fleck [2000] proposed two phenomenological isotropic constitutive models for the plastic behavior of metallic foams, and good agreement was found between their experimental results and analytical predictions. Xue et al. [2005] presented a phenomenological plastic constitutive model for compressible orthotropic materials and extended the model for applications to metal core structures in sandwich plates. This plastic constitutive model was also implemented in a finite element program to study the dynamic mechanical behavior of metal cores [Vaziri and Xue 2007]. From investigations of the representative periodic units, Gibson and Ashby [1997] presented basic mechanical results about ideal and commercial hexagonal honeycombs. Mohr [2005] suggested a mechanism-based multisurface plasticity model for ideal truss lattice materials. Standard homogenization techniques were employed to develop a general micromechanics-based finite-strain constitutive model for truss lattice materials. Wang and McDowell [2005] systematically calculated the initial yield surfaces of five different types of planar lattice patterns by analysis of the periodic unit cells, considering both the in-plane and triaxial stress states. Doyoyo and Mohr [2003] experimentally investigated the microstructural response of aluminum honeycomb under combined normal and shear out-of-plane loading. Zhang et al. [2008] designed two novel statically indeterminate planar lattice structures and calculated their initial yield surfaces and buckling surfaces.

It should be noted that the previous studies about yield surfaces of lattice structures were mainly based on numerical or experimental methods. These methods are commonly complicated and often cannot provide simple explicit results which are more convenient for engineering applications. However, it must be noted that high accuracy results can be obtained by utilizing these methods, especially for the case where buckling of the microstructure is evident. For most stretching dominated structures composed of moderately flexible struts (that is, when the relative density is larger than 0.06), comparison of the yield strengths and elastic strengths indicates that elastic buckling generally does not occur before yielding [Wang and McDowell 2004; Zhang et al. 2008]. In this case, the analytical method based on the micromechanics method, through analysis of the periodic unit cell, is capable of deriving explicit yield surface results with enough accuracy. Since the statically indeterminate lattice structure is still dominated by stretching after the initial yielding, it can still sustain comparatively large additional load after initial yielding. Besides, this category of lattices is expected to possess higher specific strengths than that of statically determinate lattices such as the triangular and Kagome lattices. Therefore, for practical applications of the statically indeterminate lattice structures in engineering conditions, it is crucial to investigate their ultimate yield behavior in detail. The results concerning the ultimate yielding of statically indeterminate cells have not been reported so far.

In this paper, a simple analytical method based on analysis of the equilibrium of the periodic unit cell before and after initial yielding is put forward to calculate the ultimate yield equations of planar lattice structures whose degree of static indeterminacy are one, which is introduced in Section 2.

In Section 3, the ultimate yield surfaces of three statically indeterminate planar lattices are calculated using this method. Comparison of yield strengths among these lattice structures are made in Section 4.

Finally, in Section 5, the whole stress-strain relationships of two statically indeterminate lattice structures in the principal directions are analyzed.

2. Formulation of ultimate yield surface

We consider a representative statically indeterminate lattice structure so that its periodic unit cell, comprised of eight struts fastened to each other, has a parallelogram shape as depicted in Figure 1. The structure undergoes in-plane deformation under multiaxial stressing. The applied normal stresses in the x_1 and x_2 directions are denoted as σ_1 and σ_2 , respectively, and the shear stress is τ_{12} . It is noted that the pair of struts having the same orientation must exhibit identical mechanical behavior, so analyzing only one strut is sufficient for each pair. For convenience, each selected strut in the four pairs is numbered by i th, $i = 1, \dots, 4$ respectively and the length of the i th strut is l_i .

The onsets of yielding of the four pairs of struts are generally not concurrent. As the applied stresses increase up to a set of particular values, a certain pair of struts starts to yield. This state is considered the *initial yielding* of the lattice structure. After initial yielding, the unit cell of the structure is still capable of withstanding further loading. Continuously increasing the loads results in at least one more pair of struts also yielding. Consequently, the structural unit cell will become a mechanism and eventually collapse. We name such behavior the *ultimate yielding* of the lattice structure. After the initial yielding of the statically indeterminate lattice structure, the load is mainly supported by the original configuration (excluding the initially yielding struts) although the initial yielding struts still increase in strength to some extent when the material possesses a strain hardening effect. The strain hardening effect of the parent material will make the solution of the ultimate yielding equation very complicated. Therefore, all struts are assumed to be made of elastic, perfectly plastic material in this paper. Basically, once the ultimate yielding occurs, the structure cannot bear additional loads any more in this case. It is also possible that

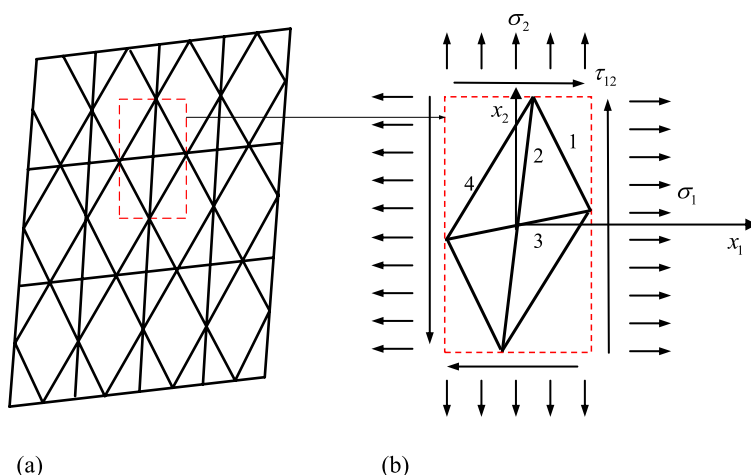


Figure 1. Sketch of a representative statically indeterminate lattice structure (a) and its unit cell (b).

two or more pairs of struts simultaneously start to yield, in which case we consider that the structure is undergoing the ultimate yielding without experiencing the initial yielding. The evolution of structural yielding will be addressed again later, while the emphasis in this section is to establish the equations for identifying the initial and ultimate yielding conditions of the structure.

According to the criteria proposed by Deshpande et al. [2001], the lattice pattern in Figure 1 is a stretching dominated structure. Furthermore, the unit cell in Figure 1 without one pair of struts is still statically determinate, and each strut still undergoes mainly stretching or compressing; that is to say, the structure is still stretching dominant after initial yielding. Therefore, the deformation of the lattice structure is still very small compared with the dimension of the lattice unit cell. The analytical results in Section 5 also demonstrate that the effective ultimate yielding strain of the lattice structures are both within $5\varepsilon_{ys}$, where ε_{ys} denotes the strain of the solid material. For the typical value of $\varepsilon_{ys} = 0.001$, for a metal material, the effective ultimate yielding strain of the lattice structure is only 0.005. Therefore, the assumption of “small deformation” is still reasonable after initial yield. The agreement of the analytical and Finite Element (FE) results on the stress-strain relationships of the SI-square and N-Kagome cells in Section 5 also demonstrate that the “small deformation” assumption can be accepted. Besides, the bending deformation of each strut in the lattice structure is still small enough so that they cannot contact each other. The results of finite element method (FEM) calculations also support this statement. As shown in Figure 2, when ultimate yielding in the SI-square lattice structure occurs under uniaxial loading in the x_1 and diagonal directions, the bending deformations and rotational angles of each strut are both comparatively small. Therefore, the assumption that the structural elements do not contact each other is precise for describing the deformation mode before the ultimate yielding of the lattice structure, and the equilibrium equations established on the original configuration of the lattice are also accurate enough.

Due to the dominance of cell wall stretching, the internal force of the i th strut is proportional to each applied stress component, thus the initial yielding condition of the i th strut can be written in nondimensional terms as

$$|N_i/(\sigma_{ys}bt)| = |p_i\sigma_1^\circ/\sigma_{ys} + q_i\sigma_2^\circ/\sigma_{ys} + r_i\tau_{12}^\circ/\sigma_{ys}| = 1, \quad i = 1, \dots, 4, \tag{1}$$

where N_i denotes the internal force of the i th strut, and σ_{ys} is the yield strength of strut material; b and t are the in-plane wall thickness and out-of-plane dimensions, respectively; σ_1° , σ_2° and τ_{12}° are the applied stresses leading to initial yielding of the unit cell. The coefficients p_i , q_i , and r_i can be considered as the contributing fraction of each stress component to the internal force of the i th strut, depending on the

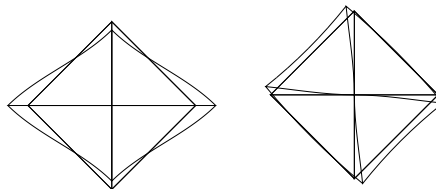


Figure 2. The deformation sketches of the SI-square cell under uniaxial loading in the x_1 and diagonal directions with the deformations magnified by 100 times.

initial structural geometry. For the case in which a single stress component exists (that is, σ_1), the related coefficient (that is, p_i) can be determined straightforwardly (that is, $p_i = N_i/(\sigma_1 bt)$).

It is noted that after initial yielding (that is, the i th strut is yielding), the structure is still stretching dominant. Assuming that the j^{th} ($j = 1, \dots, 4, j \neq i$) strut yields subsequently after the i th strut, then the corresponding ultimate yield equation of the unit cell can be given by

$$|N_j^{(i)}/(\sigma_{ys}bt)| = |(N_j^{(i)\circ} + \Delta N_j^{(i)})/\sigma_{ys}bt|$$

$$= \left| \begin{array}{l} p_j \sigma_1^\circ/\sigma_{ys} + q_j \sigma_2^\circ/\sigma_{ys} \\ + r_j \tau_{12}^\circ/\sigma_{ys} + P_j^{(i)} \Delta\sigma_1/\sigma_{ys} \\ + Q_j^{(i)} \Delta\sigma_2/\sigma_{ys} + R_j^{(i)} \Delta\tau_{12}/\sigma_{ys} \end{array} \right| = 1, \quad i, j = 1, \dots, 4, j \neq i, \quad (2)$$

where $N_j^{(i)\circ}$ denotes the internal force of the j th strut at the onset of initial yielding of the i th strut. $\Delta N_j^{(i)}$ denotes the additional internal force within the j th strut thereafter, and correspondingly $\Delta\sigma_1$, $\Delta\sigma_2$, and $\Delta\tau_{12}$ are the additional applied stresses thereafter. By definition, the additional stresses can be written by

$$\Delta\sigma_1 = \sigma_1 - \sigma_1^\circ, \quad (3)$$

$$\Delta\sigma_2 = \sigma_2 - \sigma_2^\circ, \quad (4)$$

$$\Delta\tau_{12} = \tau_{12} - \tau_{12}^\circ, \quad (5)$$

where σ_1 , σ_2 , and τ_{12} are the final applied stresses. Analogous to p_i , q_i , and r_i , the coefficients $P_j^{(i)}$, $Q_j^{(i)}$, and $R_j^{(i)}$ can be considered as the contribution fraction of each stress component increment to the additional internal force of the j th strut after the initial yielding of the structure. They are determined by the geometrical configuration, which excludes the initially yielding struts (the i th strut), and this configuration is named the postyielding configuration. Assuming that an additional stress is exerted to such postyielding configuration, ($\Delta\sigma_1$), the related coefficients (that is, $P_j^{(i)}$) can be determined straightforwardly ($P_j^{(i)} = N_j^{(i)}/(\Delta\sigma_1 bt)$).

Substituting Equation (3) into (2) gives

$$\left| \begin{array}{l} (p_j - P_j^{(i)})\sigma_1^\circ/\sigma_{ys} + (q_j - Q_j^{(i)})\sigma_2^\circ/\sigma_{ys} \\ + (r_j - R_j^{(i)})\tau_{12}^\circ/\sigma_{ys} + P_j^{(i)}\sigma_1/\sigma_{ys} \\ + Q_j^{(i)}\sigma_2/\sigma_{ys} + R_j^{(i)}\tau_{12}/\sigma_{ys} \end{array} \right| = 1, \quad i, j = 1, \dots, 4, j \neq i. \quad (6)$$

Through analyzing, in detail, the equilibrium of the structural unit cell under the specified uniaxial stressing, we find that the parameters $(p_j - P_j^{(i)})$, $(q_j - Q_j^{(i)})$, $(r_j - R_j^{(i)})$, and p_i , q_i , r_i satisfy the following generalized relation:

$$\frac{p_j - P_j^{(i)}}{p_i} = \frac{q_j - Q_j^{(i)}}{q_i} = \frac{r_j - R_j^{(i)}}{r_i} = s_j^{(i)}, \quad (i, j = 1, \dots, 4, i \neq j), \quad (7)$$

where $s_j^{(i)}$ is introduced as the scale parameter, depending only on the geometry of the unit cell. The details of the procedure for getting Equation (7) will be given in Appendix A. For the special structure depicted in Figure 1, the parameter $s_j^{(i)}$ can be further related to the length ratios. By introducing the effective lengths, defined as $l'_1 = l_1$, $l'_2 = 2l_2$, $l'_3 = 2l_3$, and $l'_4 = l_4$, $s_j^{(i)}$ can be simply written in a generalized form as

$$s_j^{(i)} = \begin{cases} l'_j/l'_i & i + j = 5, \\ -l'_j/l'_i & i + j \neq 5, \end{cases} \quad (i, j = 1, \dots, 4, i \neq j). \tag{8}$$

The term $|(p_j - P_j^{(i)})\sigma_1^\circ/\sigma_{ys} + (q_j - Q_j^{(i)})\sigma_2^\circ/\sigma_{ys} + (r_j - R_j^{(i)})\tau_{12}^\circ/\sigma_{ys}|$ can be simplified by combining Equations (1) and (7), that is,

$$\left| (p_j - P_j^{(i)})\sigma_1^\circ/\sigma_{ys} + (q_j - Q_j^{(i)})\sigma_2^\circ/\sigma_{ys} + (r_j - R_j^{(i)})\tau_{12}^\circ/\sigma_{ys} \right| = |s_j^{(i)}|. \tag{9}$$

Substituting (9) into (6), the ultimate yield equation is written as:

$$\begin{aligned} \max_{i,j=1,\dots,4,i \neq j} \{ |s_j^{(i)} + P_j^{(i)}\sigma_1/\sigma_{ys} + Q_j^{(i)}\sigma_2/\sigma_{ys} + R_j^{(i)}\tau_{12}/\sigma_{ys}| \} &= 1 \\ (\text{when } \max_{i=1,\dots,4} \{ p_i\sigma_1/\sigma_{ys} + q_i\sigma_2/\sigma_{ys} + r_i\tau_{12}/\sigma_{ys} \} &\geq 1, \quad i = 1, \dots, 4), \end{aligned} \tag{10a}$$

$$\begin{aligned} \max_{i,j=1,\dots,4,i \neq j} \{ |-s_j^{(i)} + P_j^{(i)}\sigma_1/\sigma_{ys} + Q_j^{(i)}\sigma_2/\sigma_{ys} + R_j^{(i)}\tau_{12}/\sigma_{ys}| \} &= 1 \\ (\text{when } \min_{i=1,\dots,4} \{ p_i\sigma_1/\sigma_{ys} + q_i\sigma_2/\sigma_{ys} + r_i\tau_{12}/\sigma_{ys} \} &\leq -1, \quad i = 1, \dots, 4). \end{aligned} \tag{10b}$$

Equation (10a) is related to the i th strut’s initial yielding under tension, while Equation (10b) is related to its initial yielding under compression. It should be pointed out that the above equations are applicable for any kind of statically indeterminate structures whose degrees of static indeterminacy are one even though their derivation is based on the particular configuration shown in Figure 1.

Here we make a simple comparison of the present analytical method with the methods adopted in the previous investigations on the yield surfaces of the lattice structures. Xue et al. [2005] proposed a phenomenological ellipsoidal yield surface for lattice materials based on the six initial yield strengths in the orthotropic axes. This kind of closed-form yield surface is advantageous in establishing the hardening rule and the plastic constitutive relations similar to that of the isotropic metal material. The deformation of each strut within the lattice cell is not detailed analyzed in this model, so this phenomenological method is not capable of presenting an explicit ultimate yielding equation beyond the initial yielding. Mohr [2005] suggested a mechanism-based multisurface plasticity model for ideal truss lattice materials. Standard homogenization techniques were employed to develop a general micromechanics-based finite-strain constitutive model for truss lattice materials. In their integration algorithm, an iterative numerical method needs to be adopted to check the yield condition and calculate the plastic strain step by step, and thus an explicit analytical ultimate equation also cannot be obtained using their method.

3. Ultimate yield surfaces of three types of lattice structures

Utilizing the equations presented in Section 2, we explore the ultimate yield surfaces of several lattice structures, including the diamond cross cell, SI-square cell and N-Kagome cell. The configurations of

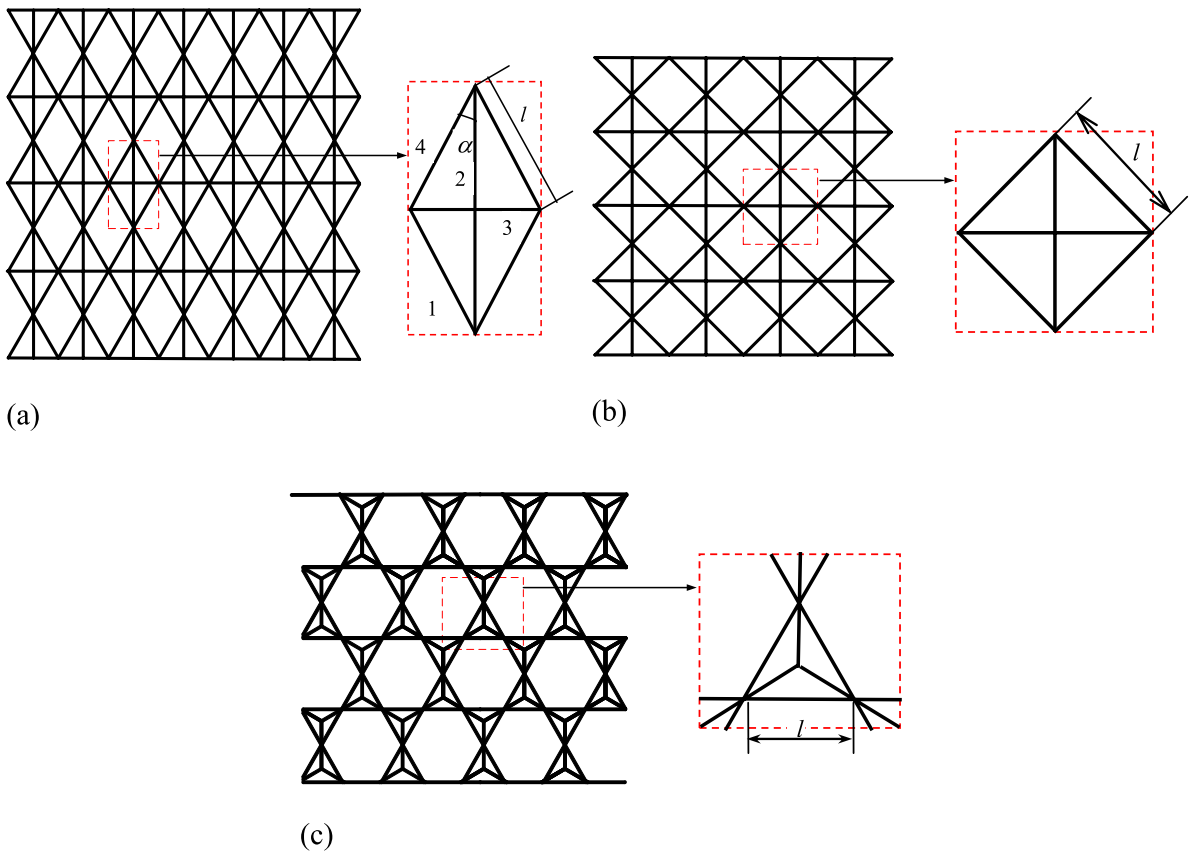


Figure 3. Configurations of the diamond cross (a), the SI-square (b), and the N-Kagome (c) lattice structures.

these lattice structures are shown in Figure 3. Figure 3(a) presents a diamond cross cell having a half top angle of α , which can be specified by setting the lengths of all four outside struts of the unit cell structure shown in Figure 1 to be equal. The statically indeterminate square (SI-square) cell, as shown in Figure 3(b), is considered to be a special diamond cross cell having the half top angle of $\alpha = \pi/4$. The N-Kagome cell, proposed by Zhang et al. [2008], is presented in Figure 3(c). Compared with the original Kagome cell, the N-Kagome cell has three short struts inside the triangle. Zhang et al. [2008] indicated that, for a given relative density and wall thickness, the N-Kagome cell has larger hexagon cavities, which are convenient for oil storage, disposal of heat exchanger, battery deploying and for other functions..

In this section, the procedure of gaining the ultimate yield surfaces is explained in detail by exemplifying that of the diamond cross cell. The similar descriptions for the SI-square and N-Kagome cells are omitted and only the results of the ultimate yield surfaces for these two cells are listed in Appendix B. By employing an energy method, the statically indeterminate problem of the diamond cross cell under a general stress state can be solved, and the internal forces of each strut can be expressed in terms of the applied stress components. Then the initial yield equation of the diamond cross cell is obtained as

follows:

$$\max \begin{bmatrix} \frac{l}{t\sigma_{ys}} \left| \frac{\sin 2\alpha(\sigma_1 \sin \alpha + \sigma_2 \cos \alpha)}{1+2 \sin^3 \alpha + 2 \cos^3 \alpha} - \tau_{12} \right| - 1 \\ \frac{l}{t\sigma_{ys}} \left| \frac{-\sigma_1 \sin^2 2\alpha + 2\sigma_2 \sin \alpha(1+2 \sin^3 \alpha)}{1+2 \sin^3 \alpha + 2 \cos^3 \alpha} \right| - 1 \\ \frac{l}{t\sigma_{ys}} \left| \frac{2\sigma_1 \cos \alpha(1+2 \cos^3 \alpha) - \sigma_2 \sin^2 2\alpha}{1+2 \sin^3 \alpha + 2 \cos^3 \alpha} \right| - 1 \\ \frac{l}{t\sigma_{ys}} \left| \frac{\sin 2\alpha(\sigma_1 \sin \alpha + \sigma_2 \cos \alpha)}{1+2 \sin^3 \alpha + 2 \cos^3 \alpha} + \tau_{12} \right| - 1 \end{bmatrix} = 0. \tag{11}$$

According to Equation (8), the values of $s_j^{(i)}$ are calculated and written in form of an array as following,

$$[s_j^{(i)}] = \begin{bmatrix} / & -2 \cos \alpha & -2 \sin \alpha & 1 \\ -\frac{1}{2 \cos \alpha} & / & \frac{\sin \alpha}{\cos \alpha} & -\frac{1}{2 \cos \alpha} \\ -\frac{1}{2 \sin \alpha} & \frac{\cos \alpha}{\sin \alpha} & / & -\frac{1}{2 \sin \alpha} \\ 1 & -2 \cos \alpha & -2 \sin \alpha & / \end{bmatrix}, \tag{12}$$

where i and j are the row index and column index, respectively and $i \neq j$.

Based on the methods briefed in the previous section, the parameters, $P_j^{(i)}$, $Q_j^{(i)}$, and $R_j^{(i)}$, are identified by

$$[P_j^{(i)}] = \begin{bmatrix} / & 0 & 2bl \cos \alpha & 0 \\ 0 & / & 2bl \cos \alpha & 0 \\ bl \frac{\cos \alpha}{\sin \alpha} & -2bl \frac{\cos^2 \alpha}{\sin \alpha} & / & bl \frac{\cos \alpha}{\sin \alpha} \\ 0 & 0 & 2bl \cos \alpha & / \end{bmatrix}, \quad [Q_j^{(i)}] = \begin{bmatrix} / & 2bl \sin \alpha & 0 & 0 \\ bl \frac{\sin \alpha}{\cos \alpha} & / & -2bl \frac{\sin^2 \alpha}{\cos \alpha} & 0 \\ 0 & 2bl \sin \alpha & / & 0 \\ 0 & 2bl \sin \alpha & 0 & / \end{bmatrix},$$

$$[R_j^{(i)}] = \begin{bmatrix} / & 0 & -2bl \cos \alpha & -2bl \cos \alpha \\ -bl & / & 2bl \cos \alpha & bl \\ -bl & 0 & / & bl \\ -2bl & 2bl \cos \alpha & 2bl \sin \alpha & / \end{bmatrix}. \tag{13}$$

Substituting Equations (11), (12) and (13) into Equations (10a) and (10b) gives the ultimate yield equations of the diamond cross cell, that is,

$$\max \left[\begin{array}{l} 2\frac{l}{t\sigma_{ys}} |-\sin \alpha + \sigma_1 \cos \alpha \pm \tau_{12} \sin \alpha| - 1 \\ 2\frac{l}{t\sigma_{ys}} |-\cos \alpha + \sigma_2 \sin \alpha \pm \tau_{12} \cos \alpha| - 1 \\ \frac{l}{t\sigma_{ys}} |1 \pm 2\tau_{12} \cos \alpha| - 1 \\ \frac{l}{t\sigma_{ys}} \left| \frac{\sin \alpha}{\cos \alpha} + 2\sigma_1 \cos \alpha - 2\sigma_2 \frac{\sin^2 \alpha}{\cos \alpha} \right| - 1 \\ \frac{l}{t\sigma_{ys}} \left| \frac{\cos \alpha}{\sin \alpha} - 2\sigma_1 \frac{\cos^2 \alpha}{\sin \alpha} + 2\sigma_2 \sin \alpha \right| - 1 \end{array} \right] = 0, \quad \text{when}$$

$$\max \left[\begin{array}{l} \frac{l}{t\sigma_{ys}} \frac{\sin 2\alpha(\sigma_1 \sin \alpha + \sigma_2 \cos \alpha)}{1 + 2\sin^3 \alpha + 2\cos^3 \alpha} - \tau_{12} - 1 \\ \frac{l}{t\sigma_{ys}} \frac{-\sigma_1 \sin^2 2\alpha + 2\sigma_2 \sin \alpha(1 + 2\sin^3 \alpha)}{1 + 2\sin^3 \alpha + 2\cos^3 \alpha} - 1 \\ \frac{l}{t\sigma_{ys}} \frac{2\sigma_1 \cos \alpha(1 + 2\cos^3 \alpha) - \sigma_2 \sin^2 2\alpha}{1 + 2\sin^3 \alpha + 2\cos^3 \alpha} - 1 \\ \frac{l}{t\sigma_{ys}} \frac{\sin 2\alpha(\sigma_1 \sin \alpha + \sigma_2 \cos \alpha)}{1 + 2\sin^3 \alpha + 2\cos^3 \alpha} + \tau_{12} - 1 \end{array} \right] > 0, \quad (14a)$$

$$\max \left[\begin{array}{l} 2\frac{l}{t\sigma_{ys}} |\sin \alpha + \sigma_1 \cos \alpha \pm \tau_{12} \sin \alpha| - 1 \\ 2\frac{l}{t\sigma_{ys}} |\cos \alpha + \sigma_2 \sin \alpha \pm \tau_{12} \cos \alpha| - 1 \\ \frac{l}{t\sigma_{ys}} |-1 \pm 2\tau_{12} \cos \alpha| - 1 \\ \frac{l}{t\sigma_{ys}} \left| -\frac{\sin \alpha}{\cos \alpha} + 2\sigma_1 \cos \alpha - 2\sigma_2 \frac{\sin^2 \alpha}{\cos \alpha} \right| - 1 \\ \frac{l}{t\sigma_{ys}} \left| -\frac{\cos \alpha}{\sin \alpha} - 2\sigma_1 \frac{\cos^2 \alpha}{\sin \alpha} + 2\sigma_2 \sin \alpha \right| - 1 \end{array} \right] = 0, \quad \text{when}$$

$$\min \left[\begin{array}{l} -\frac{l}{t\sigma_{ys}} \frac{\sin 2\alpha(\sigma_1 \sin \alpha + \sigma_2 \cos \alpha)}{1 + 2\sin^3 \alpha + 2\cos^3 \alpha} - \tau_{12} + 1 \\ -\frac{l}{t\sigma_{ys}} \frac{-\sigma_1 \sin^2 2\alpha + 2\sigma_2 \sin \alpha(1 + 2\sin^3 \alpha)}{1 + 2\sin^3 \alpha + 2\cos^3 \alpha} + 1 \\ -\frac{l}{t\sigma_{ys}} \frac{2\sigma_1 \cos \alpha(1 + 2\cos^3 \alpha) - \sigma_2 \sin^2 2\alpha}{1 + 2\sin^3 \alpha + 2\cos^3 \alpha} + 1 \\ -\frac{l}{t\sigma_{ys}} \frac{\sin 2\alpha(\sigma_1 \sin \alpha + \sigma_2 \cos \alpha)}{1 + 2\sin^3 \alpha + 2\cos^3 \alpha} + \tau_{12} + 1 \end{array} \right] < 0. \quad (14b)$$

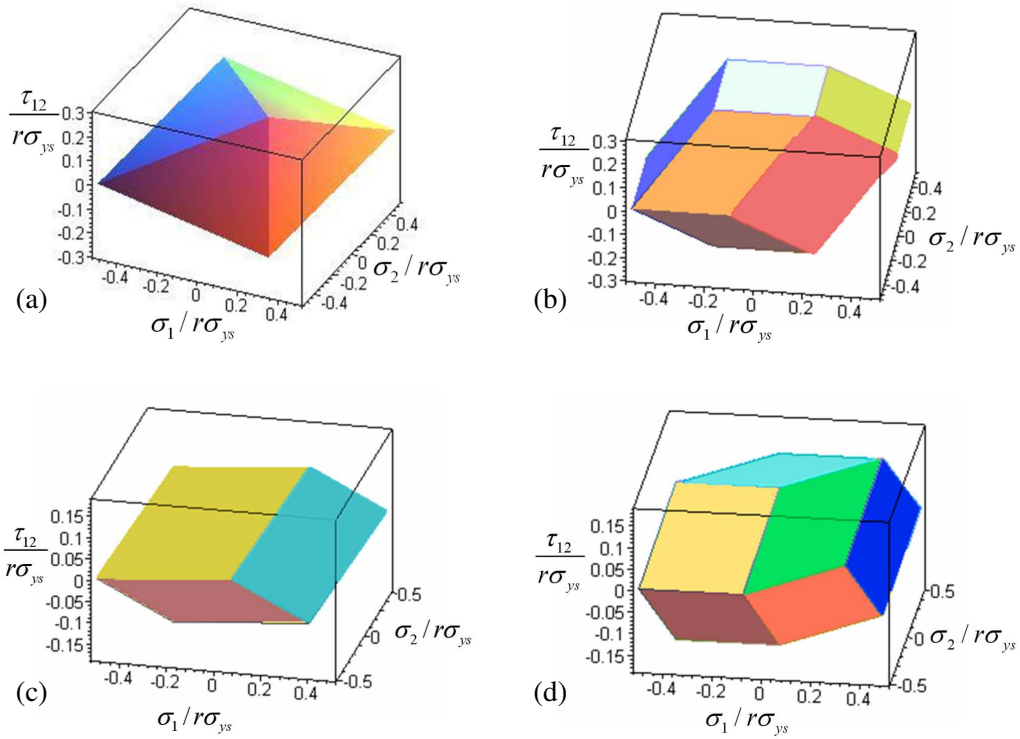


Figure 4. The initial (a) and ultimate (b) yield surfaces of the SI-square cell, and the initial (c) and ultimate (d) yield surfaces of the N-Kagome cell.

Since the SI-square lattice structure can be considered as a special diamond cross lattice structure, only the results for the SI-square and N-Kagome lattice structures are discussed herein. Figures 4(a) and 4(b) show the initial and ultimate yield surfaces of the SI-square cell in the space of normalized effective stresses respectively, while Figures 4(c) and 4(d) are corresponding to the N-Kagome cell. All four yield surfaces are closed, convex, and anisotropic. By comparison, the ultimate yield surfaces of both structures are entirely outside their initial yield surfaces, indicating that the structures still have capabilities of bearing extra loads after the onset of initial yielding. It is also demonstrated that the magnitude of the residual carrying capacity depends on the loading conditions. The initial and ultimate yield surfaces consist of only planar facets. This is the common feature of the stretching dominated structures.

Representations of yield surfaces in the stress spaces of σ_1 and σ_2 , σ_1 and τ_{12} , and σ_2 and τ_{12} are illustrated in Figures 5(a), (b) and (c) respectively. In all three stress spaces, the ultimate yield surfaces of the SI-square cell embrace those of the N-Kagome cell with a large extra area, although the sizes of their initial yield surfaces are comparative with those of the N-Kagome cell. Therefore, we may draw a conclusion that the SI-square cell has much larger ultimate load-carrying capacity than the N-Kagome cell.

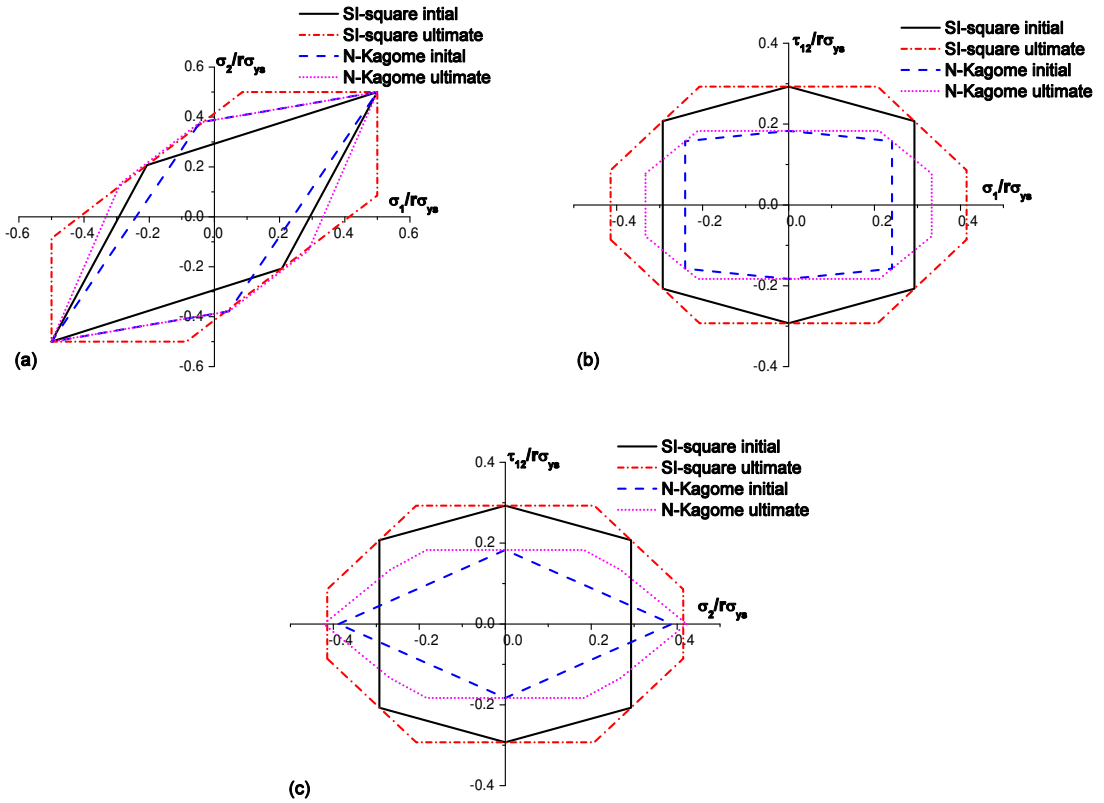


Figure 5. The initial and ultimate yield surfaces of the SI-square cell and N-Kagome cell in the stress spaces of σ_1, σ_2 (a), σ_1, τ_{12} (b) and σ_2, τ_{12} (c).

4. Yielding responses of the lattice structures under uniaxial loading

In order to estimate the structural load carrying capacity, we analyze the ultimate yield strength of each aforementioned lattice patterns subjected to uniaxial loads. Assume that the angle between the loading direction and x_1 direction is θ ($0 \leq \theta < \pi$). The resultant stress can be decomposed into two normal stress components and a shear stress component such that

$$\sigma_1 = \sigma \cos^2 \theta, \quad \sigma_2 = \sigma \sin^2 \theta, \quad \tau_{12} = \sigma \sin \theta \cos \theta. \quad (15)$$

Thus, the ultimate yield equations obtained before can be easily exploited to calculate the yielding responses of the structures to given stresses in any loading directions.

4.1. The ultimate yield strengths of three lattice structures under uniaxial loading. From (14a), (14b), and (15), the ultimate yield strength of the diamond cross cell related to the loading direction of θ is

obtained as

$$\frac{\sigma_{ut}^*(\theta)}{\sigma_{ys}} = \min \left[\begin{array}{c} \left| \frac{\sin \alpha + \cos \alpha}{2 \cos^2 \theta \cos^2 \alpha - 2 \sin^2 \theta \sin^2 \alpha} \frac{t}{l} \right| \\ \left| \frac{1}{\sin \theta \cos \theta} \frac{t}{l} \right| \\ \left| \frac{1 + 2 \sin \alpha}{2 \cos \theta \cos(\alpha \pm \theta)} \frac{t}{l} \right| \\ \left| \frac{1 + 2 \cos \alpha}{2 \sin \theta \cos(\alpha \pm \theta)} \frac{t}{l} \right| \end{array} \right]. \tag{16}$$

For the SI-square cell, its ultimate yield strength as a function of θ is given by

$$\frac{\sigma_{ut}^*(\theta)}{\sigma_{ys}} = \begin{cases} \frac{\sqrt{2}-1}{\cos 2\theta} r & (0 \leq \theta \leq 0.0541\pi), \\ \frac{1}{2 \cos \theta (\sin \theta + \cos \theta)} r & (0.0541\pi \leq \theta \leq \frac{\pi}{4}). \end{cases} \tag{17}$$

where r is the relative density of the lattice structure. Furthermore, the values of the maximum and minimum ultimate yield strengths for the SI-square cell are as follows,

$$\frac{\sigma_{ut \max}^*}{\sigma_{ys}} = 0.5r, \quad \left(\theta = \frac{n\pi}{2} \pm \frac{\pi}{4}, n = 1, \dots, 4 \right), \tag{18a}$$

$$\frac{\sigma_{ut \min}^*}{\sigma_{ys}} = 0.414r, \quad \left(\theta = \frac{n\pi}{2}, n = 1, \dots, 4 \right). \tag{18b}$$

For the N-Kagome cell, the relationship between the ultimate strength and the loading direction is calculated according to the ultimate yield equation (Equation (A.4)), that is,

$$\frac{\sigma_{ut}^*(\theta)}{\sigma_{ys}} = \begin{cases} \frac{r}{4 \cos^2 \theta - 1} & (0 \leq \theta < \frac{\pi}{12}), \\ \frac{(\sqrt{3}-1)r}{\sqrt{3} \cos 2\theta + \sin 2\theta} & (\frac{\pi}{12} \leq \theta < \frac{\pi}{6}), \\ 0.388r & (\theta = \frac{\pi}{6}). \end{cases} \tag{19}$$

Its maximum and minimum values of normalized ultimate strengths are given by

$$\frac{\sigma_{ut \max}^*}{\sigma_{ys}} = 0.423r, \quad \theta = \frac{n\pi}{3} + \frac{\pi}{6} (n = 0, \dots, 5), \tag{20a}$$

$$\frac{\sigma_{ut \min}^*}{\sigma_{ys}} = 0.333r, \quad \theta = \frac{n\pi}{3} + \frac{\pi}{3} (n = 0, \dots, 5). \tag{20b}$$

4.2. Comparison of yield strength for various cell patterns. The yield strengths of four types of cell patterns, including the diamond, Kagome, SI-square, and diamond cross cells, are compared in Figure 6. Among them, the former two, as representatives of the statically determinate lattice structures, are excellent structures for high specific stiffness and specific strength [Wang and McDowell 2004; 2005]. Different from the SI-square and diamond cross cells, they are not able to sustain further load after initial yielding. Therefore, their initial yield strengths are adopted to identify their maximum load-carrying capability. For the latter two statically indeterminate structures, the SI-square and diamond cross cells, the

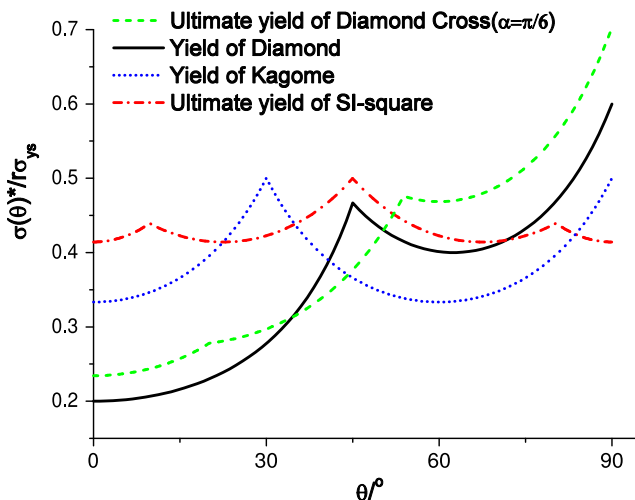


Figure 6. Comparison of yield strength among four different cell patterns.

ultimate yield strengths are employed to weigh their maximum load-carrying capabilities. The diamond cross cell that we analyze has the half top angle of $\alpha = \pi/6$. Basically, the yield strengths of the structures vary as the loading direction changes. The ultimate yield strength of the SI-square cell stays at a higher level relative to that of the Kagome cell over almost the whole range of loading directions, indicating that the SI-square cell has an advantage with respect to withstanding loads. For both the diamond and diamond cross cells, their strengths depend on the applied loading direction. The minimum yield strengths of both patterns occur when $\theta = 0^\circ$ while the maximum values are higher than 0.6 at $\theta = 90^\circ$. On the whole, the ultimate yield strengths of the diamond cross cell ($\alpha = \pi/6$) are slightly higher than that of the diamond cell. It is usual in estimation of the structural performance to adopt the worst case scenario so that the structure is considered to be a better one if it is able to survive relatively longer under any loading conditions. By comparison, the SI-square cell, the minimum yield strength of which is much higher than the others, is recommended as the best two-dimensional lattice structure for its superior load carrying capability among those aforementioned lattice patterns.

For the diamond cross cell with different half top angle α , the uniaxial ultimate yield strength is also calculated and plotted in Figure 7. It is noted that if rotated an angle of $\pi/2$, the diamond cross cell of the half top angle α will be the same as that of the half top angle $\pi/2 - \alpha$. Therefore, the top angle considered in the analysis is restricted in the range of $0 < \alpha \leq \pi/4$. As shown in Figure 7, as the half top angle decreases from $\pi/7$, the maximum yield strength is elevated and the minimum yield strength is lowered slightly. Therefore, the structure exhibits more obvious anisotropy. When the half top angle α is less than $\pi/6$, each of the corresponding curves is composed of three segments, and value of the normalized strength $(\sigma_{ut}^*(\theta)/\sigma_y)(1/r)$ increases with load direction θ . For α in the range of $\pi/6 < \alpha < \pi/4$, the corresponding curve consists of four parts. It is noted that the anisotropy of the structural response is not always a disadvantage. Particularly, for the case where the applied load is fixed at a determined direction, the half top angle of the structure can be well designed to ensure that its corresponding yield strength is as high as possible. The structure with the half top angle of $\pi/4$ evolves into the SI-square one, which displays a more isotropic yielding behavior.

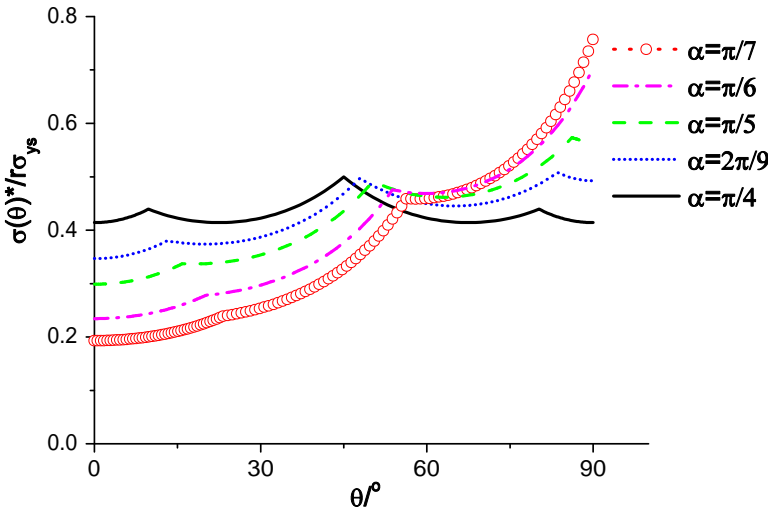


Figure 7. The ultimate yield strength of the diamond cross cells with different half top angles.

4.3. Evolution of the yield modes for the SI-square cell. As discussed before, the SI-square cell, as a statically indeterminate structure, undergoes initial yielding followed by the ultimate yielding. Its initial yield strength and ultimate yield strength are presented in Figure 8 as a function of θ . As the loading direction θ varies, both the initial yield strength and the ultimate yield strength are changed. It is seen that there exist several sharp peaks on the curves. Careful analysis exposes that each sharp peak actually corresponds to the transition of the yielding modes from one to another. Corresponding to each marked point on the curves, the yield modes are demonstrated in Figure 8. The curved segment between *A* and *E* on the initial yield curve arises from the fact that the horizontal struts experience yielding; the curved segment between *E* and *F* is related to the case where the inclined struts yield first. Initial yielding of a pair of struts usually does not mark the limit of its load-carrying resistance. Rather, it signifies a change in the way in which the structure responds to further loads. The structural unit cell does not collapse until additional plastic yielding struts have formed to convert it into a mechanism. The collapse modes are different for different loading directions. For $\theta = 0^\circ$, after the horizontal struts yield initially, the vertical struts will yield finally as the applied effective stress increases up to $\sigma^*(\theta)/r\sigma_{ys} = 0.414$. For either $\theta = 9.7^\circ$ or $\theta = 45^\circ$, three pairs of struts, including the horizontal, the vertical, and the inclined struts, all yield together once the applied load increases beyond the corresponding values of the ultimate yield strength. It is also noted that at $\theta = 27.3^\circ$ the horizontal and inclined struts will yield simultaneously, resulting in direct structural collapse without initial yielding. The maximum load carrying capacity of the SI-square structure occurs when the load is applied to the unit cell along the angle of $\theta = 45^\circ$, while the structure is relatively weaker to the horizontally applied load.

5. Stiffness analysis under uniaxial loading

For the struts made of the elastic, perfectly plastic material, the stress-strain relationships and stiffness characteristics of the SI-square and N-Kagome cells are also solved analytically and presented in this section.

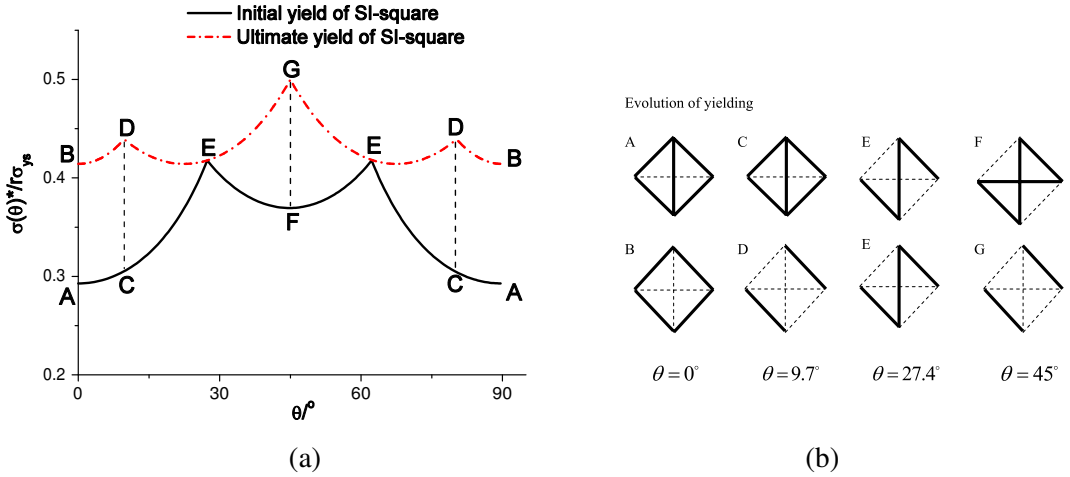


Figure 8. The initial and ultimate yield strength of the SI-square cell (a) along with the evolution of the yielding mode (b).

Considering the stress-strain relationship of the SI-square cell loaded in the x_1 direction ($\theta = 0^\circ$), with increase of the effective stress, σ_1 , from zero to the initial yield strength, the effective stress is proportional to the effective strain, with the slope just equal to the effective modulus. If the stress still increases after the initial yielding, the horizontal strut will yield (see yielding mode A in Figure 8), and the additional stress, $\Delta\sigma_1$, will be proportional to the additional strain $\Delta\varepsilon_1$. In this case, the stress is still linearly dependent on the strain, while the slope becomes the effective modulus of the unit cell without the horizontal strut. This is presented in Figure 9. The second pair of struts will occur yielding when the stress reaches the ultimate yield strength. After onset of the ultimate yielding, the unit cell is not able to support additional stress any more. The effective modulus and initial yield strength of the SI-square cell have been obtained by Zhang et al. [2008]. The effective stiffness of the unit cell without the initial yielding strut can also be easily calculated, thus the normalized stress-strain relationship can be gained, that is,

$$\frac{\sigma_1}{r\sigma_{ys}} = \begin{cases} \frac{2-\sqrt{2}}{2} \frac{\varepsilon_1}{\varepsilon_{ys}}, & 0 \leq \frac{\varepsilon_1}{\varepsilon_{ys}} \leq 1, \\ \frac{2-\sqrt{2}}{2} + \frac{3-2\sqrt{2}}{2} \left(\frac{\varepsilon_1}{\varepsilon_{ys}} - 1\right), & 1 < \frac{\varepsilon_1}{\varepsilon_{ys}} \leq \sqrt{2} + 1, \\ \sqrt{2} - 1, & \frac{\varepsilon_1}{\varepsilon_{ys}} > \sqrt{2} + 1, \end{cases} \quad (21)$$

where ε_{ys} is the yield strain of the material, and the stiffness of the material is $E_s = \sigma_{ys}/\varepsilon_{ys}$. Similarly, the normalized stress-strain relationship of the SI-square cell in the diagonal direction can also be obtained,

$$\frac{\sigma_{diag}}{r\sigma_{ys}} = \begin{cases} \frac{4-\sqrt{2}}{7} \frac{\varepsilon_{diag}}{\varepsilon_{ys}}, & 0 \leq \frac{\varepsilon_{diag}}{\varepsilon_{ys}} \leq 1, \\ \frac{4-\sqrt{2}}{7} + \frac{5\sqrt{2}-6}{14} \left(\frac{\varepsilon_{diag}}{\varepsilon_{ys}} - 1\right), & 1 < \frac{\varepsilon_{diag}}{\varepsilon_{ys}} \leq \frac{4+\sqrt{2}}{2}, \\ \frac{1}{2}, & \frac{\varepsilon_{diag}}{\varepsilon_{ys}} > \frac{4+\sqrt{2}}{2}. \end{cases} \quad (22)$$

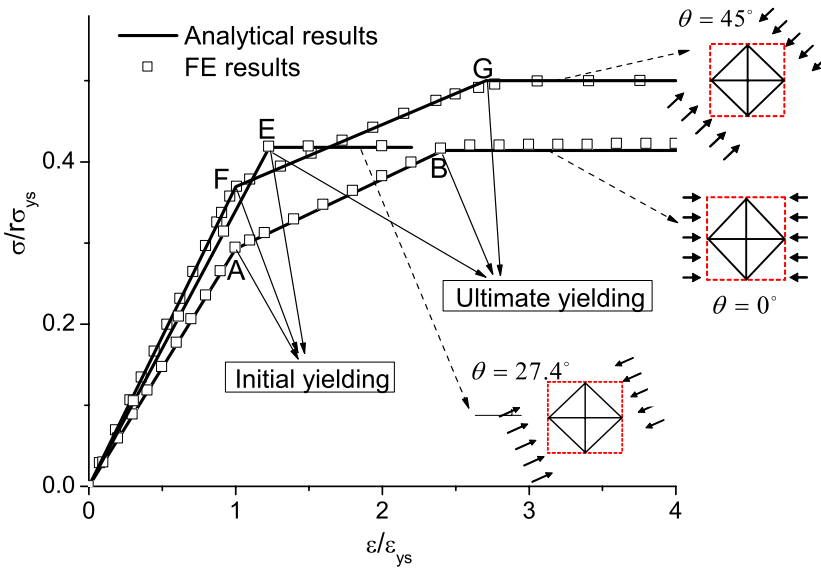


Figure 9. The stress-strain relationships of the SI-square cell in the three typical directions.

The normalized stress-strain relationship of the N-Kagome cell in the x_1 and x_2 directions could also be calculated,

$$\frac{\sigma_1}{r\sigma_{ys}} = \begin{cases} \frac{9-2\sqrt{3}}{23} \frac{\epsilon_1}{\epsilon_{ys}}, & 0 \leq \frac{\epsilon_1}{\epsilon_{ys}} \leq 1, \\ \frac{9-2\sqrt{3}}{23} + \frac{11\sqrt{3}-15}{138} \left(\frac{\epsilon_1}{\epsilon_{ys}} - 1 \right), & 1 < \frac{\epsilon_1}{\epsilon_{ys}} \leq \frac{9+2\sqrt{3}}{3}, \\ \frac{1}{3}, & \frac{\epsilon_1}{\epsilon_{ys}} > \frac{9+2\sqrt{3}}{3}. \end{cases} \quad (23)$$

$$\frac{\sigma_2}{r\sigma_{ys}} = \begin{cases} \frac{9-2\sqrt{3}}{23} \frac{\epsilon_2}{\epsilon_{ys}}, & 0 \leq \frac{\epsilon_2}{\epsilon_{ys}} \leq \frac{16+\sqrt{3}}{11}, \\ \frac{6-\sqrt{3}}{11} + \frac{111-45\sqrt{3}}{694} \frac{\epsilon_2}{\epsilon_{ys}}, & \frac{16+\sqrt{3}}{11} < \frac{\epsilon_2}{\epsilon_{ys}} \leq 2.345, \\ \frac{3-\sqrt{3}}{3}, & \frac{\epsilon_2}{\epsilon_{ys}} > 2.345. \end{cases} \quad (24)$$

According to Equations (21)–(24), the normalized stress-normalized strain curves are plotted in Figures 9 and 10 for the SI-square and the N-Kagome cells respectively. Each change in slope corresponds to the formation of plastic struts which produces progressive flexibility of the structure. In Figure 9, each marked transition point is corresponding to the yielding mode marked with the same letter in Figure 8. Collapse occurs when enough struts have undergone plastic yielding to transform the structure into a mechanism with no inherent stiffness, corresponding to the final horizontal segments of the curves.

Corresponding FE simulations are performed to verify the analytical stress-strain relations. In the calculation, the material is linear elastic with linear hardening plasticity. A small linearly hardening coefficient, $E'/E = 0.001$, is adopted for the cell wall material, where E and E' are the elastic modulus

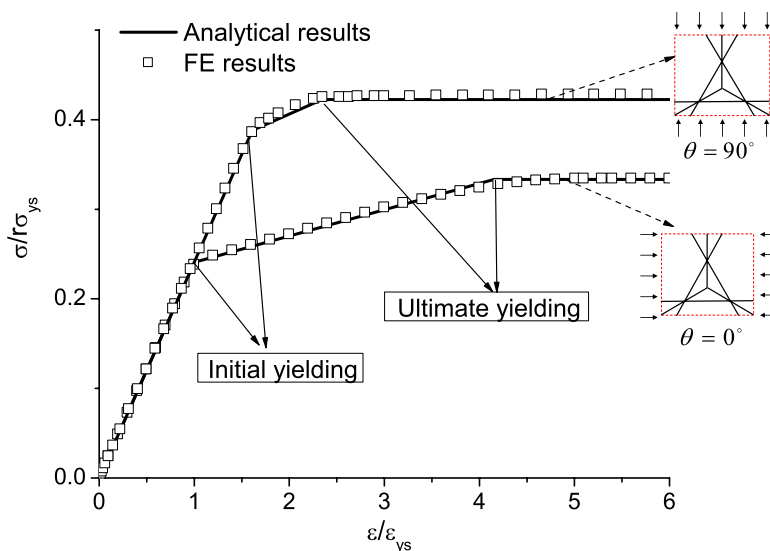


Figure 10. The stress-strain relationships of the N-Kagome cell in the principle directions.

and the tangential modulus. As shown in Figures 9 and 10, good agreements are found between the FE results and the analytical stress-strain predictions, thus verifying the analytical solutions.

6. Concluding remarks

Based on the analysis of the equilibrium of a unit cell before and after initial yielding, a simple analytical method is put forward to calculate the ultimate yield equation of statically indeterminate planar lattice structures for the elastic, perfectly plastic parent material. The ultimate yield surfaces and yield strengths of several indeterminate unit cells are assessed using the proposed method, and the residual loading capacity after the onset of initial yielding can be quantitatively predicted. The stress-strain relationships of the SI-square and N-Kagome cells are also calculated for the elastic, perfectly plastic materials, and the effective constitutive relations of both lattices are found to be linearly hardening, which is validated by finite element (FE) simulations. Comparison of the initial and ultimate yield surfaces indicates that these lattice structures possess considerable residual loading capacities which depend on the loading conditions. It is found that the ultimate yield strength of the SI-square cell is nearly isotropic, possesses a higher ultimate yield strength, and therefore is an excellent lightweight structure for load carrying. The ultimate yield strengths of the diamond cross cell ($\alpha = \pi/6$) are slightly higher than that of the diamond cell on the whole.

Appendix A: the deduction of the relationship given by Equation (7)

In order to obtain the relationships between the parameters $(p_j - P_j^{(i)})$, $(q_j - Q_j^{(i)})$, $(r_j - R_j^{(i)})$, and p_i , q_i , r_i , the equilibrium of the unit cell is analyzed. The anticlockwise angle of the i th strut and the x_1 direction is assumed to be θ_i . For the case where the first strut yields first, that is, $i = 1$, we simply take the values of applied stresses to be unit, that is, $\sigma_1 = 1$ or $\Delta\sigma_1 = 1$, which can be equivalent to two

concentrated loads exerted on the connecting nodes of the struts, P_A and P_B , as shown in Figure 11. (We note that the stress quantities σ and $\Delta\sigma$ are reference stresses that can be chosen arbitrarily; they are simply scaling factors.) The equilibrium equations of points A and B before initial yielding are

$$\begin{aligned} -p_1 \cos \theta_1 + p_3 \cos \theta_3 + p_4 \cos \theta_4 &= P_A/bt, \\ -p_1 \sin \theta_1 + p_3 \sin \theta_3 + p_4 \sin \theta_4 &= 0, \\ p_1 \sin \theta_1 + p_2 \sin \theta_2 + p_4 \sin \theta_4 &= 0, \\ p_1 \cos \theta_1 + p_2 \cos \theta_2 + p_4 \cos \theta_4 &= -P_B/bt. \end{aligned} \tag{A.1}$$

The equilibrium equations of points A and B after initial yielding are:

$$\begin{aligned} P_3^{(1)} \cos \theta_3 + P_4^{(1)} \cos \theta_4 &= P_A/bt, \\ P_3^{(1)} \sin \theta_3 + P_4^{(1)} \sin \theta_4 &= 0, \\ P_2^{(1)} \sin \theta_2 + P_4^{(1)} \sin \theta_4 &= 0, \\ P_2^{(1)} \cos \theta_2 + P_4^{(1)} \cos \theta_4 &= -P_B/bt. \end{aligned} \tag{A.2}$$

Subtracting each equation of Equation (A.2) from Equation (A.1) gives:

$$\begin{aligned} (p_3 - P_3^{(1)}) \cos \theta_3 + (p_4 - P_4^{(1)}) \cos \theta_4 &= p_1 \cos \theta_1, \\ (p_3 - P_3^{(1)}) \sin \theta_3 + (p_4 - P_4^{(1)}) \sin \theta_4 &= p_1 \sin \theta_1, \\ (p_2 - P_2^{(1)}) \sin \theta_2 + (p_4 - P_4^{(1)}) \sin \theta_4 &= -p_1 \sin \theta_1, \\ (p_2 - P_2^{(1)}) \cos \theta_2 + (p_4 - P_4^{(1)}) \cos \theta_4 &= -p_1 \cos \theta_1. \end{aligned} \tag{A.3}$$

Taking these parameters, $(p_2 - P_2^{(1)})$, $(p_3 - P_3^{(1)})$, $(p_4 - P_4^{(1)})$ and p_1 , as unknown quantities, the rank of the coefficient matrix of Equation (A.3) is three, which indicates that those four equations in Equation (A.3) are not independent, and the value of $\frac{p_j - P_j^{(1)}}{p_1}$ ($j = 2, 3, 4$) can be uniquely determined as follows,

$$\frac{p_2 - P_2^{(1)}}{p_1} = \frac{\sin(\theta_4 - \theta_1)}{\sin(\theta_2 - \theta_4)}, \quad \frac{p_3 - P_3^{(1)}}{p_1} = \frac{\sin(\theta_4 - \theta_1)}{\sin(\theta_4 - \theta_3)}, \quad \frac{p_4 - P_4^{(1)}}{p_1} = \frac{\sin(\theta_1 - \theta_3)}{\sin(\theta_4 - \theta_3)}. \tag{A.4}$$

Analogously, if the first strut yields first, and only the unit applied stress $\sigma_2 = 1$ or $\tau_{12} = 1$ exists, the following relationships can be obtained:

$$\frac{q_2 - Q_2^{(1)}}{q_1} = \frac{\sin(\theta_4 - \theta_1)}{\sin(\theta_2 - \theta_4)}, \quad \frac{q_3 - Q_3^{(1)}}{q_1} = \frac{\sin(\theta_4 - \theta_1)}{\sin(\theta_4 - \theta_3)}, \quad \frac{q_4 - Q_4^{(1)}}{q_1} = \frac{\sin(\theta_1 - \theta_3)}{\sin(\theta_4 - \theta_3)}, \tag{A.5}$$

$$\frac{r_2 - R_2^{(1)}}{r_1} = \frac{\sin(\theta_4 - \theta_1)}{\sin(\theta_2 - \theta_4)}, \quad \frac{r_3 - R_3^{(1)}}{r_1} = \frac{\sin(\theta_4 - \theta_1)}{\sin(\theta_4 - \theta_3)}, \quad \frac{r_4 - R_4^{(1)}}{r_1} = \frac{\sin(\theta_1 - \theta_3)}{\sin(\theta_4 - \theta_3)}. \tag{A.6}$$

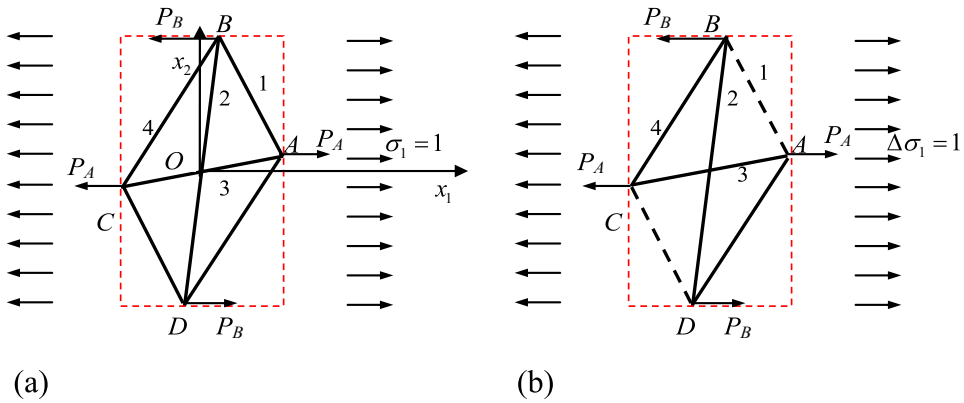


Figure 11. The unit cell under uniaxial compression in the x_1 direction (a) before and (b) after the initial yield of the first strut.

Similar deduction can be performed for the cases that the second, third, and fourth struts yield first by using the same method, and the results can be concluded as:

$$\frac{p_j - P_j^{(i)}}{p_i} = \frac{q_j - Q_j^{(i)}}{q_i} = \frac{r_j - R_j^{(i)}}{r_i} = s_j^{(i)} = \begin{cases} l'_j/l'_i & i + j = 5, \\ -l'_j/l'_i & i + j \neq 5, \end{cases} \quad (i, j = 1, \dots, 4, i \neq j), \quad (\text{A.7})$$

where the definition of $s_j^{(i)}$ and l'_i can be seen in Section 2.

Appendix B: the initial and ultimate yield equations of the SI-square and N-Kagome lattice structures

The SI-square cell can be considered as a special diamond cross cell having the half top angle of $\alpha = \pi/4$. By taking $\alpha = \pi/4$ in Equation (11) and Equation (14), the initial and ultimate yield equations of the SI-square cell are respectively given by

$$\max \begin{bmatrix} (|(\sigma_1/r\sigma_{ys} + \sigma_2/r\sigma_{ys}) - (2 + \sqrt{2})(\tau_{12}/r\sigma_{ys})| - 1), \\ (|-\sqrt{2}\sigma_1/r\sigma_{ys} + (2 + \sqrt{2})(\sigma_2/r\sigma_{ys})| - 1), \\ (|(\sigma_1/r\sigma_{ys} + \sigma_2/r\sigma_{ys}) + (2 + \sqrt{2})(\tau_{12}/r\sigma_{ys})| - 1), \\ (|(2 + \sqrt{2})(\sigma_1/r\sigma_{ys}) - \sqrt{2}(\sigma_2/r\sigma_{ys})| - 1) \end{bmatrix} = 0, \quad (\text{A.1})$$

$$\max \left[\begin{array}{l} |2(\frac{\sigma_1}{r\sigma_{ys}} + \frac{\tau_{12}}{r\sigma_{ys}})| - 1 = 0, \\ |2(\frac{\sigma_1}{r\sigma_{ys}} - \frac{\tau_{12}}{r\sigma_{ys}})| - 1 = 0, \\ |(\sqrt{2} + 1)(\frac{\sigma_1}{r\sigma_{ys}} - \frac{\sigma_2}{r\sigma_{ys}})| - 1 = 0, \\ |2(\frac{\sigma_2}{r\sigma_{ys}} + \frac{\tau_{12}}{r\sigma_{ys}})| - 1 = 0, \\ |2(\frac{\sigma_2}{r\sigma_{ys}} - \frac{\tau_{12}}{r\sigma_{ys}})| - 1 = 0, \\ |(\sqrt{2} + 2)\frac{\tau_{12}}{r\sigma_{ys}}| - 1 = 0 \end{array} \right] = 0, \tag{A.2}$$

where r is the relative density of the SI-square lattice, that is, $r = (2 + \sqrt{2})t/l$.

Exploiting the method introduced in Section 2, the initial and ultimate yield equations of the N-Kagome cell are respectively obtained as follows:

$$\max \left[\begin{array}{l} |-\frac{\sqrt{3}}{3}\frac{\sigma_1}{r\sigma_{ys}} + \frac{6+\sqrt{3}}{3}\frac{\sigma_2}{r\sigma_{ys}} - 2(1 + \sqrt{3})\frac{\tau_{12}}{r\sigma_{ys}}| - 1 \\ |-\frac{\sqrt{3}}{3}\frac{\sigma_1}{r\sigma_{ys}} + \frac{6+\sqrt{3}}{3}\frac{\sigma_2}{r\sigma_{ys}} + 2(1 + \sqrt{3})\frac{\tau_{12}}{r\sigma_{ys}}| - 1 \\ |\frac{9+2\sqrt{3}}{3}\frac{\sigma_1}{r\sigma_{ys}} - \frac{3+2\sqrt{3}}{3}\frac{\sigma_2}{r\sigma_{ys}}| - 1 \end{array} \right] = 0, \tag{A.3}$$

$$\max \left[\begin{array}{l} |2\frac{\sigma_2}{r\sigma_{ys}} - 2\sqrt{3}\frac{\tau_{12}}{r\sigma_{ys}}| - 1 \\ |2\frac{\sigma_2}{r\sigma_{ys}} + 2\sqrt{3}\frac{\tau_{12}}{r\sigma_{ys}}| - 1 \\ 2(\sqrt{3} + 1)|\frac{\tau_{12}}{r\sigma_{ys}}| - 1 \\ |-3\frac{\sigma_1}{r\sigma_{ys}} + \frac{\sigma_2}{r\sigma_{ys}}| - 1 \\ \frac{\sqrt{3}+1}{2}|\sqrt{3}(-\frac{\sigma_1}{r\sigma_{ys}} + \frac{\sigma_2}{r\sigma_{ys}}) - 2\frac{\tau_{12}}{r\sigma_{ys}}| - 1 \\ \frac{\sqrt{3}+1}{2}|\sqrt{3}(-\frac{\sigma_1}{r\sigma_{ys}} + \frac{\sigma_2}{r\sigma_{ys}}) + 2\frac{\tau_{12}}{r\sigma_{ys}}| - 1 \end{array} \right] = 0, \tag{A.4}$$

where the relative density of the N-Kagome cell is $r = (\sqrt{3} + 1)\frac{t}{l}$.

References

[Ashby et al. 2000] M. F. Ashby, A. G. Evans, N. A. Fleck, L. J. Gibson, J. W. Hutchinson, and H. N. G. Wadley, *Metal foams: a design guide*, Butterworth Heinemann, Boston, 2000.

[Chen et al. 1999] C. Chen, T. J. Lu, and N. A. Fleck, “Effect of imperfections on the yielding of two-dimensional foams”, *J. Mech. Phys. Solids* **47** (1999), 2235–2272.

[Deshpande and Fleck 2000] V. S. Deshpande and N. A. Fleck, “Isotropic constitutive models for metallic foams”, *J. Mech. Phys. Solids* **48** (2000), 1253–1283.

- [Deshpande et al. 2001] V. S. Deshpande, M. F. Ashby, and N. A. Fleck, “Foam topology bending versus stretching dominated architectures”, *Acta Mater.* **49** (2001), 1035–1040.
- [Doyoyo and Mohr 2003] M. Doyoyo and D. Mohr, “Microstructural response of aluminum honeycomb to combined out-of-plane loading”, *Mech. Mater.* **35** (2003), 865–876.
- [Doyoyo and Wierzbicki 2003] M. Doyoyo and T. Wierzbicki, “Experimental studies on the yield behavior of ductile and brittle aluminum foams”, *Int. J. Plast.* **19** (2003), 1195–1214.
- [Evans et al. 2001] A. G. Evans, J. W. Hutchinson, N. A. Fleck, M. F. Ashby, and H. N. G. Wadley, “The topological design of multifunctional cellular metals”, *Prog. Mater. Sci.* **46** (2001), 309–327.
- [Fazekas et al. 2002] A. Fazekas, R. Dendievel, L. Salvo, and Y. Brechet, “Effect of microstructural topology upon the stiffness and strength of 2D cellular structures”, *Int. J. Mech. Sci.* **44** (2002), 2047–2066.
- [Fleck and Qiu 2007] N. A. Fleck and X. M. Qiu, “The damage tolerance of elastic-brittle, two-dimensional isotropic lattices”, *J. Mech. Phys. Solids* **55** (2007), 562–588.
- [Gibson and Ashby 1997] L. J. Gibson and M. F. Ashby, *Cellular solids: structure and properties*, 2nd Edition ed., Cambridge Uni. Press, Cambridge, 1997.
- [Hayes et al. 2004] A. M. Hayes, A. Wang, B. M. Dempsey, and D. L. McDowell, “Mechanics of linear cellular alloys”, *Mech. Mater.* **36** (2004), 691–713.
- [Hutchinson and Xue 2005] J. W. Hutchinson and Z. Xue, “Metal sandwich plates optimized for pressure impulses”, *Int. J. Mech. Sci.* **47** (2005), 545–569.
- [Mohr 2005] D. Mohr, “Mechanism-based multi-surface plasticity model for ideal truss lattice materials”, *Int. J. Solids Struct.* **42** (2005), 3235–3260.
- [Smith et al. 2001] H. B. Smith, J. W. Hutchinson, and A. G. Evans, “Measurement and analysis of the structural performance of cellular metal sandwich construction”, *Int. J. Mech. Sci.* **43** (2001), 1945–1963.
- [Vaziri and Xue 2007] A. Vaziri and Z. Xue, “Mechanical behavior and constitutive modeling of metal cores”, *J. Mech. Mater. Struct.* **2** (2007), 1743–1760.
- [Wang and McDowell 2004] A. J. Wang and D. L. McDowell, “In-plane stiffness and yield strength of periodic metal honeycombs”, *J. Eng. Mater. Technol. (Trans. ASME)* **126** (2004), 137–156.
- [Wang and McDowell 2005] A. J. Wang and D. L. McDowell, “Yield surfaces of various periodic metal honeycombs at intermediate relative density”, *Int. J. Plast.* **21** (2005), 285–320.
- [Xue and Hutchinson 2003] Z. Xue and J. W. Hutchinson, “Preliminary assessment of sandwich plates subject to blast loads”, *Int. J. Mech. Sci.* **45** (2003), 687–705.
- [Xue and Hutchinson 2004] Z. Xue and J. W. Hutchinson, “A comparative study of impulse-resistant metal sandwich plates”, *Int. J. Impact Eng.* **30** (2004), 1283–1305.
- [Xue and Hutchinson 2006] Z. Xue and J. W. Hutchinson, “Crush dynamics of square honeycomb sandwich cores”, *Int. J. Numer. Methods Eng.* **65** (2006), 2221–2245.
- [Xue et al. 2005] Z. Xue, A. Vaziri, and J. W. Hutchinson, “Non-uniform hardening constitutive model for compressible orthotropic materials with application to sandwich plate cores”, *Comput. Model. Eng. Sci.* **10** (2005), 79–95.
- [Zhang et al. 2008] Y. H. Zhang, X. M. Qiu, and D. N. Fang, “Mechanical properties of two novel planar lattice structures”, *Int. J. Solids Struct.* **45** (2008), 3751–3768.

Received 3 Jan 2008. Revised 30 May 2008. Accepted 4 Jun 2008.

YIHUI ZHANG: zhang-yh06@mails.tsinghua.edu.cn

Department of Engineering Mechanics FML, Tsinghua University, Beijing, 100084, China

ZHENYU XUE: xue@seas.harvard.edu

Department of Engineering Mechanics FML, Tsinghua University, Beijing, 100084, China

XINMING QIU: qxm@mail.tsinghua.edu.cn

Department of Engineering Mechanics FML, Tsinghua University, Beijing, 100084, China

DAINING FANG: fangdn@mail.tsinghua.edu.cn

Department of Engineering Mechanics FML, Tsinghua University, Beijing, 100084, China

